



1 Article

2 Computational Predictions and Microwave Plasma

Synthesis of Superhard Boron-Carbon Materials

- 4 Paul A. Baker, Shane A. Catledge, Sumner B. Harris, Kathryn J. Ham, Wei-Chih Chen,
- 5 Cheng-Chien Chen, and Yogesh K. Vohra*
- 6 Department of Physics, University of Alabama at Birmingham (UAB), Birmingham, AL 35294, USA
- 7 * Correspondence: ykvohra@uab.edu; Tel.: +1-205-934-6662
- 8 Received: date; Accepted: date; Published: date

Abstract: Superhard boron-carbon materials are of prime interest due to their non-oxidizing properties at high temperatures as compared to diamond-based materials and their non-reactivity with ferrous metals under extreme conditions. In this work, evolutionary algorithms combined with density functional theory have been utilized to predict stable structures and properties for the boron-carbon system including the elusive superhard BC5 compound. We report on the microwave plasma chemical vapor deposition on a silicon substrate of a series of composite materials containing amorphous boron-doped graphitic carbon, boron-doped diamond, and a cubic hard-phase with a boron-content as high as 7.7 at%. The nanoindentation hardness of these composite materials can be tailored from 8 GPa to as high as 62 GPa depending on the growth conditions. These materials have been characterized by electron microscopy, x-ray photoelectron spectroscopy, Raman spectroscopy, x-ray diffraction, and nanoindentation hardness and experimental results are compared with theoretical predictions. Our studies show that a significant amount of boron up to 7.7 at% can be accommodated in the cubic phase of diamond and its phonon modes and mechanical properties can be accurately modeled by theory. This cubic hard-phase can be incorporated into amorphous boron-carbon matrices to yield superhard materials with tunable hardness values.

Keywords: Boron-carbon compound, superhard materials, ab initio calculations, chemical vapor deposition.

2627

28

29

30

31

32

33

34

35

36

37

38

39

40

41

42

43

44

9

10

11

12

13

14

15

16

17

18

19

20

21

22

23

24

25

1. Introduction

The first row of elemental solids (C, N, O, and B—jointly referred to as CNOB) form dense covalent solids in three-dimensional (3D) network structures that are extremely hard, have high-energy density content, and exhibit unique electronic and optical properties. While diamond (hardness of approx. 100 GPa) and cubic-boron nitride (hardness of approx. 45 GPa) have long been established as the cornerstone of a multi-billion dollar abrasives industry, there is considerable scientific and technological interest in novel superhard materials (hardness greater than 40 GPa) based on CNOB. Low pressure/low-temperature synthesis affords metastable development of unique superhard binary, ternary, and quaternary phases from CNOB precursors that can be quenched to form conformal coatings on a large range of substrates.

In this paper, we focus on a sub-set of superhard materials based on the boron-carbon system where synthesis of superhard BC $_5$ material has previously been claimed using the high-pressure high-temperature technique at a pressure of 24 GPa and temperature of about 2200 K [1]. The synthesized BC $_5$ material had a measured hardness value of 71 GPa and high thermal stability up to 1900 K [1]. Subsequently, a significant amount of theoretical work has suggested various stable and metastable superhard modifications of boron-carbon systems [2-9]. Our previous study of low-level boron incorporation in diamond by microwave plasma chemical vapor deposition showed a

significant change in the plasma gas-phase chemistry and morphology of the diamond films by the introduction of boron in a methane/hydrogen/nitrogen plasma [10]. The focus of this work is on the synthesis of metastable superhard boron-carbon composites from the gas phase using low-temperature microwave plasma chemical vapor deposition. The advantage of microwave plasma chemical vapor deposition (CVD) is its ability for large area synthesis and for overcoming limitations of high-pressure high-temperature techniques. We have employed gas phase precursors based on hydrogen (H₂), methane (CH₄), and diborane (B₂H₆) in materials synthesis using a microwave plasma source.

2. Materials and Methods

The silicon substrates were obtained from pieces of a <100> oriented, N/Ph doped silicon wafer (University Wafer #1095). These were ultrasonically cleaned with solvents, scratched with diamond powder (2-4µm particle size) for 30 seconds on a polishing pad, and then ultrasonically cleaned with DI water and methanol to remove any diamond particles. The B-C films were grown using a 6 kW microwave plasma chemical vapor deposition reactor on a silicon substrate using hydrogen/methane/diborane chemistry. The deposition conditions were: 500 standard cubic centimeters per minute (SCCM) H₂ as the carrier gas, 22 SCCM CH₄ as the carbon source, and 0.1-0.45 SCCM B₂H₆ as the boron source and substrate temperature was carefully controlled in the range of 750 °C to 950 °C. The first 45 min of each deposition was performed with only the methane as the precursor to deposit a layer of microcrystalline diamond and the diborane was added to the plasma for synthesis of high-boron content superhard boron-carbon composites. The deposition conditions are outlined in Table I for the four samples described in this manuscript.

Sample	Growth temp. (°C)	Microwave power (W)	Chamber pressure	CH ₄ (SCCM)	B ₂ H ₆ (SCCM)	Growth time hrs. (diamond/B-C)
			(Torr)			
LBDD	875	900	58	22	residual	5.5 hrs/N-A
HBDD	845	850	51	22	0.15	2/2.8
SBCC	925	900	60	22	0.15	0.75/6.3
HBCC	775	850	53	22	0.45	0.77/6.8

Table I: Growth conditions for the four samples described in this study. The nomenclature of samples is as follows LBDD = lightly boron-doped diamond, HBDD = heavily boron-doped diamond, SBCC = soft boron-carbon composite, and HBCC = hard boron-carbon composite

The films were analyzed with a Phi Electronics Versaprobe 5000, equipped with a micro-focused Al monochromatic source (λ =1486.6 eV) and a dual anode conventional x-ray source with a neutralizer. The Mg anode provides X-rays of energy 1253.6 eV and the survey spectra were taken with a pass energy of 187.85 eV and a step size of 0.5 eV. Spectra were calibrated such that the C1s peak position was at 284.5 eV. A Panalytical Empyrean X-ray diffractometer was used to obtain diffraction patterns of the films. The optics used were a hybrid monochromator ($K\alpha$ 1=1.54059 Å) with a 1/8° divergence slit and a parallel plate collimator on the diffracted beam path with a proportional detector. The films were imaged with a FEI QuantaTM 650 FEG scanning electron microscope. The micro-Raman spectrometer is a Dilor XY with an input laser of 532nm.

Hardness and Young's modulus were measured using a NanoIndenter XP having a Berkovich diamond tip with nominal radius of 50 nm. A common and valid concern is in regard to blunting of the indenter diamond tip when performing hardness measurements on superhard materials. Therefore, in our measurements, we performed calibration of the indenter area function before and after hardness measurements on B-C thin films. A fused silica calibration standard (accepted Young's modulus of 72 GPa) was tested before and after testing of each CVD-grown sample. All samples, including silica, were indented to a maximum depth of 400 nm. The measured Young's modulus and hardness values were determined at maximum load and averaged from 10-15 indents (for silica sample) with uncertainty represented as standard deviation of the data. Young's modulus

90

91

92

93

94

95

96

97

98

99

100

101

102

103

104

105

106

107

108

109

110

111

112

113

114

115

116

117

118

119

120

121

122

123

124

125

126

127

128

129

130

131

132

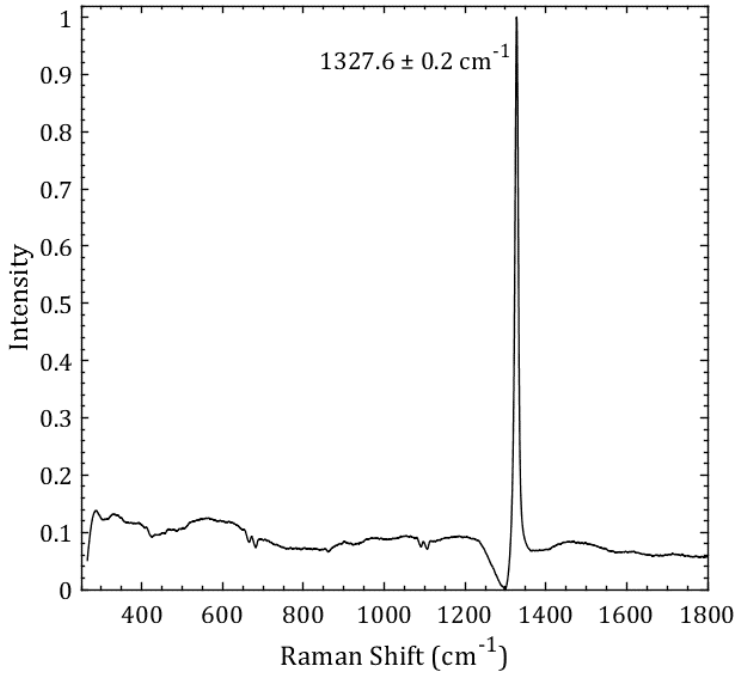
of the silica before and after testing all CVD-grown samples was 73.3 ± 0.6 GPa and 74.8 ± 0.9 GPa, respectively. Therefore, the Young's modulus of the silica calibration standard remained within 4 percent of its average starting value and the indenter tip area function was not modified throughout all tests.

We have performed crystal structure predictions to study stable superhard BC $_5$ structures. In principle one would like to find the stable structure of a compound knowing only its chemical formula by locating the minimum of the Gibbs free energy G = U + PV - TS. It is much more involved to compute the entropy and temperature effects, so quite often only the enthalpy H = U + PV is minimized in practice. The minima of the potential energy surface correspond to different stable and metastable structures, which could potentially be stabilized under different experimental conditions.

The crystal structure prediction is performed using the USPEX (Universal Structure Predictor: Evolutionary Xtallography) software [11-13] based on an evolutionary algorithm developed by Oganov, Glass, Lyakhov and Zhu. This stochastic method uses concepts such as survival of the fittest and mutation inspired by biological evolution to locate the global minimum of a potential energy surface. The implementation of the algorithm features local optimization, real-space representation, and flexible physically motivated variation operators for highly efficient and accurate structure generation and prediction. For BC₅, we consider unit cells containing two formula units (12 atoms) and search for the lowest-enthalpy structures in the pressure range 0-75 GPa with a 5 GPa interval. Among the superhard phases of BC5 we found, we then perform additional structure relaxation calculation at zero pressure to locate the lowest-energy structures, which is a widely used procedure in structure prediction calculation. The ab initio electronic structure calculation is performed using the VASP (Vienna Ab initio Simulation Package) program [14-15]. VASP adopts a plane wave basis set and a pseudopotential method. In our calculations, a plane wave cutoff energy of 600 eV is used, and the projector augmented wave method [16-17] with the PBE/GGA exchange correlation functional [18] is employed. The Γ-centered 22x22x5 k-point sampling in the Brillouin zone by the Monkhorst-Pack method [19] is used to calculate the total energy summation. For self-consistent and structure relaxation calculations, an energy difference less than 10-6 eV/unit-cell is set for the electronic loop convergence criterion. All structures are relaxed until the forces on each ion are smaller than 10⁻³ eV/Å. The phonon calculations are performed with the density functional perturbation theory method [20] with a 2x2x2 supercell. An energy difference less than 10-8 eV/unit-cell and forces on each ion less than 10-7 eV/Å are used for the convergence criteria. The resulting interatomic force constants provide inputs for the PHONOPY [21] code to calculate the phonon dispersions and density of states. The lattice parameter calculations for boron-doped cubic diamond were carried out with 16x16x16 k-point sampling. Single unit cells were used for 0%, and 12.5% boron concentrations, a 2x2x2 supercell was used for 1.563%, 3.125%, 4.688%, 6.25%, and 9.375 data points. It is noted that the 0% case overestimates the lattice constant of pure diamond to 3.5716 Å, about a 0.14% error from the accepted value of 3.5667 Å. We also use VASP to compute the elastic modulus tensor, from which the bulk and shear moduli can be calculated, and then the Vickers hardness can be estimated using Chen's model [22].

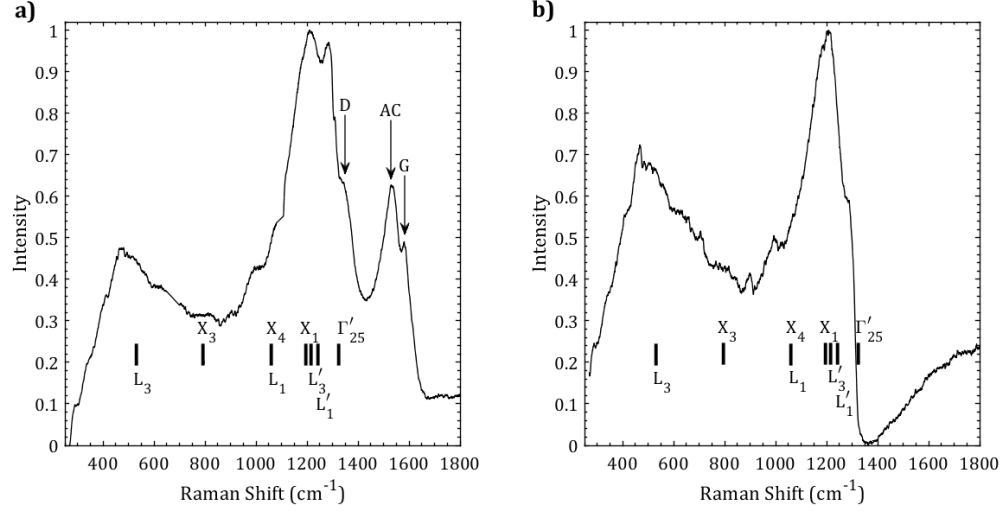
3. Results

Figure 1 shows the Raman spectrum of a lightly boron-doped diamond film (sample LBDD in Table I). The Raman spectrum is dominated by a single zone-center mode at 1327.6 cm⁻¹ and has a downward shift from a pure cubic diamond peak at 1332.5 cm⁻¹. The additional weak features that are observed in Figure 1 are attributed to the Fano effect in boron-doped diamond literature [23-24].



<u>Figure 1</u>: The measured Raman spectrum from a lightly boron-doped diamond (sample LBDD) recorded with the 532 nm laser excitation. A zone-center Raman mode at 1327.6 cm⁻¹ is accompanied by weak bands attributed to Fano effect.

The higher boron-carbon films can be divided into two distinct categories: the ones that are grown at temperatures higher than 900 °C and the ones that are grown below 850 °C. The high temperature grown films above 900 °C contain amorphous boron-doped graphite (soft-phase) while the films grown below 850 °C mostly contain superhard boron-carbon phases. Figure 2(a) shows the Raman spectrum from the film grown at 925 °C (sample SBCC in Table I) showing Raman peaks labeled "D" and "G" attributed to amorphous boron-doped graphitic carbon and a peak attributed to amorphous carbon (AC) as well as broad bands attributed to heavily boron-doped diamond. Figure 2(b) shows the Raman spectrum of a sample grown at 775 °C (sample HBCC) where boron-doped graphitic carbon and amorphous carbon peaks are completely absent.



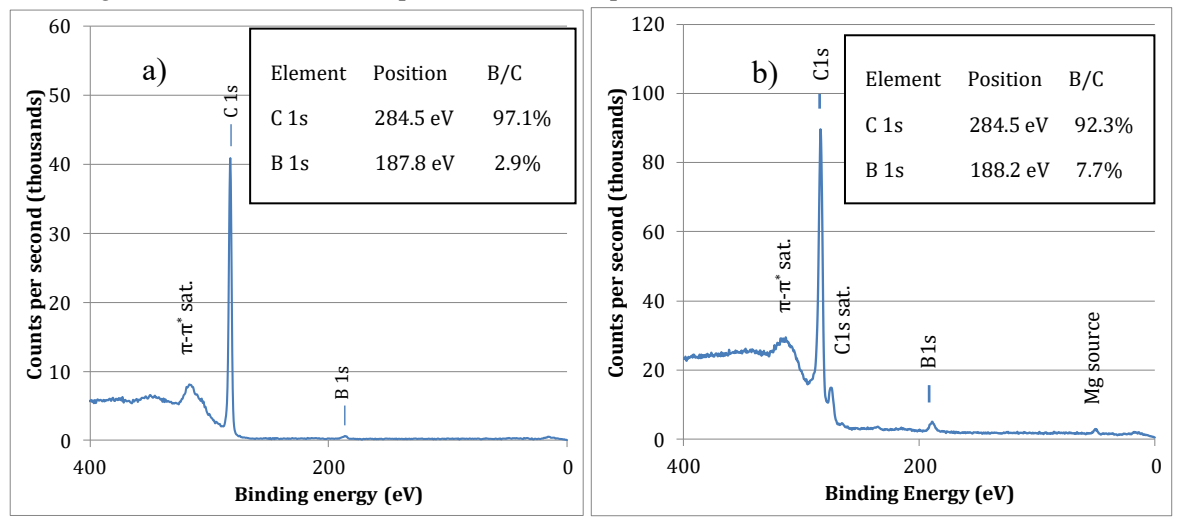
<u>Figure 2</u>: (a) Raman spectrum from sample SBCC showing "D" and "G" bands attributed to microcrystalline boron-doped graphite, amorphous carbon (AC). (b) Raman spectrum from sample HBCC showing a hard cubic-phase. The vertical bars show the location of phonon modes in cubic diamond as determined by neutron scattering experiments [25]. The observed Raman modes in boron-carbide are considerably shifted from the cubic diamond positions.

In Figure 2, we have also indicated the location of phonon modes observed in cubic diamond by neutron scattering [25], however, our observed modes are shifted downward in frequency due to addition of boron in the lattice. The measured Raman frequencies are shown in Table II and will be compared with the theoretical calculations described later in this paper.

=======								
Sample	Peak 1	Peak 2	Peak 3	Peak 4	Peak 5	Peak 6	Peak 7	Peak 8
	(cm ⁻¹)							
SBCC	463.9	684.8	1084.8	1209.6	1287.1	1346.1	1530.0	1587.3
	± 2.0	± 17.4	± 14.4	± 2.9	± 0.5	± 5.8	± 1.1	± 1.0
НВСС	466.7	705.8	1078.5	1208.2	1290.9		_	_
	± 2.1	± 29.0	± 8.3	± 0.8	± 0.5	_		
LBDD	_	_		_	1327.6	_	_	_
			_		± 0.2			
Theory	508.6	702.2	1174.7	1209.3	1294.7	_	_	

Table II: Measured Raman Frequencies of spectra shown in Figure 1 and Figure 2

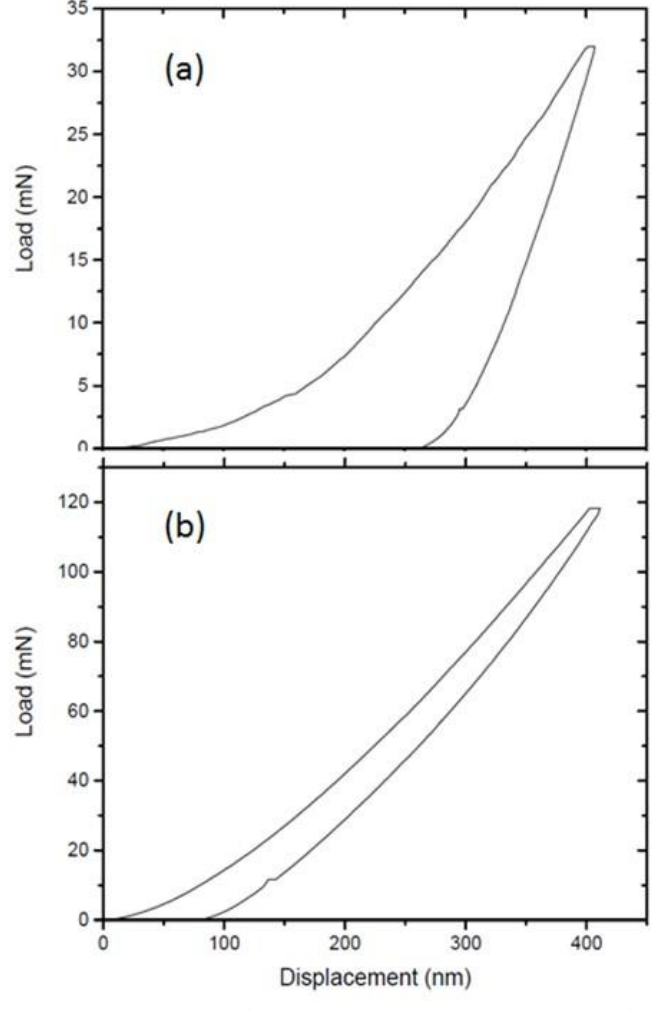
Figure 3 shows X-ray Photoelectron Spectroscopy (XPS) of the boron-carbon film grown with low and high boron content. XPS is primarily used to quantify the boron-content in the film by comparing the intensity of B 1s peak to the C 1s peak. In Figure 3(a) the boron-carbon film contains 2.9 at% boron and 97.1 at% carbon (sample HBDD in Table I), and in Figure 3(b) the sample contains 7.7 at% boron and 92.3 at% carbon (sample HBCC in Table I). The value of 2.9% boron-doping for HBDD is consistent with the heavily boron-doped samples in the literature while the 7.7 at% boron is the highest level of boron incorporation in our experiments.



<u>Figure 3</u>: The X-ray Photoelectron Spectroscopy (XPS) analysis of the two boron-carbon films where Raman spectra have been presented in Fig. 2. The composition of the film is determined from the intensities of B 1s and C1s emission intensities. (a) HBDD sample and (b) HBCC sample. The satellite (sat) peaks associated with C1s emission are also labeled.

Figure 4 shows the nanoindentation hardness measurements on samples grown at high and low temperatures. Figure 4(a) shows a load-displacement curve for soft-sample SBCC grown at high temperatures containing microcrystalline boron-doped graphite indented to a depth of 400 nm. The measured hardness (H) and Young's modulus (E) of the soft-sample is H = 7.8 GPa and E = 174 GPa, respectively. Figure 4(b) shows a load-displacement curve for hard-sample HBCC grown at low temperatures indented to a depth of 400 nm. The measured hardness and Young's modulus of the hard-sample is H = 62 GPa and E = 532 GPa, respectively. The relative contribution of elastic and plastic deformation can be calculated from the final unloading depth of the load-displacement

curves. The soft sample (SBCC) shows an elastic contribution of 35% and the hard sample (HBCC) shows an elastic contribution of as high as 79%.



<u>Figure 4</u>: The load displacement curves for the two samples to a depth of 400 nm. (a) SBCC sample showing considerable plastic deformation and yields a hardness value H = 7.8 GPa and Elastic Modulus E = 174 GPa based on two such indents and (b) HBCC sample showing minimal plastic deformation and yields a hardness value H = 61.7 GPa and Elastic Modulus E = 532 GPa based on seven such indents.

Figure 5 shows the high-resolution thin-film x-ray diffraction pattern of the B-C samples recorded with a monochromatic Cu $K_{\alpha 1}$ radiation with a wavelength of λ = 1.5406 Å. The diffraction patterns are indexed to a mixture of two cubic phases as indicated by the splitting of (111) diffraction peaks with increasing boron-content. For the HBCC samples, cubic phases with lattice parameters a_1 = 3.5743 Å and a_2 = 3.5917 Å are recorded. The lattice parameter a_1 corresponds to the underlying cubic-diamond phase and the lattice parameter a_2 corresponds to the boron-doped hard phase. It should be added that no additional super-lattice x-ray diffraction peaks were observed in addition to the two cubic-phases as documented above.

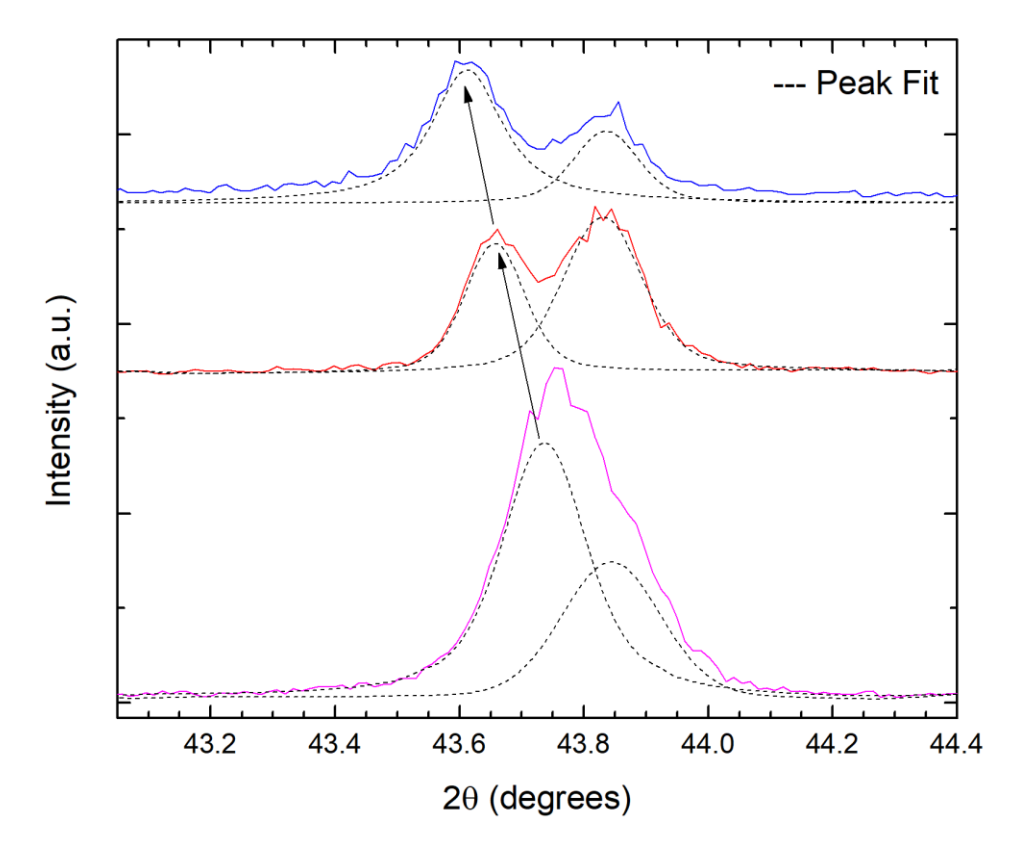


Figure 5: High resolution x-ray diffraction pattern recorded on various B-C films using a hybrid monochromator showing increased splitting of the cubic-diamond (111) diffraction peak with increasing boron-content. The boron-doped diamond peak shift to lower 2θ angles as indicated by arrows showing an increase in lattice parameter with increasing boron content.

Figure 6 shows scanning electron micrographs (SEM) of various morphologies observed in our films. Figure 6(a) shows a typical morphology of HBDD sample (2.9at% boron) where (100) cubic growth morphology is apparent in the micrograph. Figure 6(b) shows a needle like morphology amorphous boron-doped graphitic carbon (sample SBCC) where x-ray diffraction does not show crystalline graphite confirming the amorphous nature of the deposit. Figure 6(c) shows surface morphology of the sample containing 7.7at% boron (sample HBCC). This morphology shows less faceted structure than the HBDD sample, possibly indicative of increased crystalline defects (e.g. twinning).

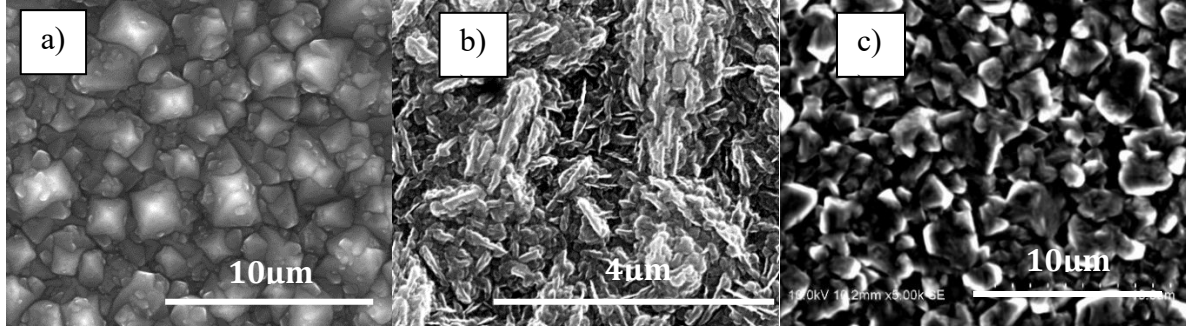
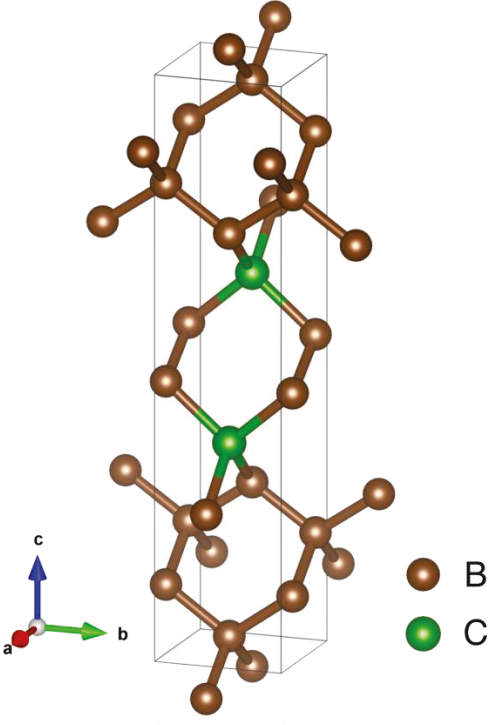


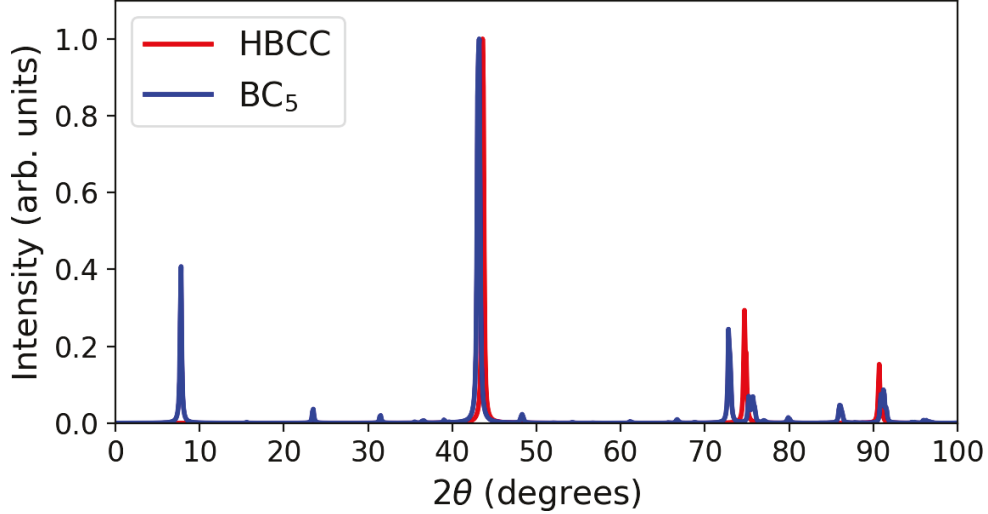
Figure 6: Scanning Electron Micrograph (SEM) of various boron-carbon composites synthesized in this study. (a) SEM of HBDD sample (2.9 at% boron) showing (100) morphology, (b) SEM of the SBCC sample containing microcrystalline boron-doped graphite, (c) SEM of the HBCC sample.

Among the superhard structures we found, the orthorhombic BC₅ (containing two formula units) with Pmma symmetry as shown in Figure 7 has the lowest energy [6]. Its fully relaxed lattice parameters a, b, and c are, respectively, 2.5103, 2.5251, and 11.373 Å. The volume is thereby 6.0076 ų/atom. The bulk and shear moduli are computed to be 378 GPa and 382 GPa, respectively, which yields a Vickers hardness H = 63 GPa for the structure in Figure 7 using the Chen's model [22]. In general, similar hardness values are obtained using other hardness models [26-27].



<u>Figure 7</u>: The lowest-energy structure of superhard BC₅ (containing two formula units) predicted by the evolutionary algorithm as implemented in USPEX [13,14,15]. The unit cell is orthorhombic with Pmma symmetry. The lattice parameters are described in the text. The predicted hardness is 63 GPa.

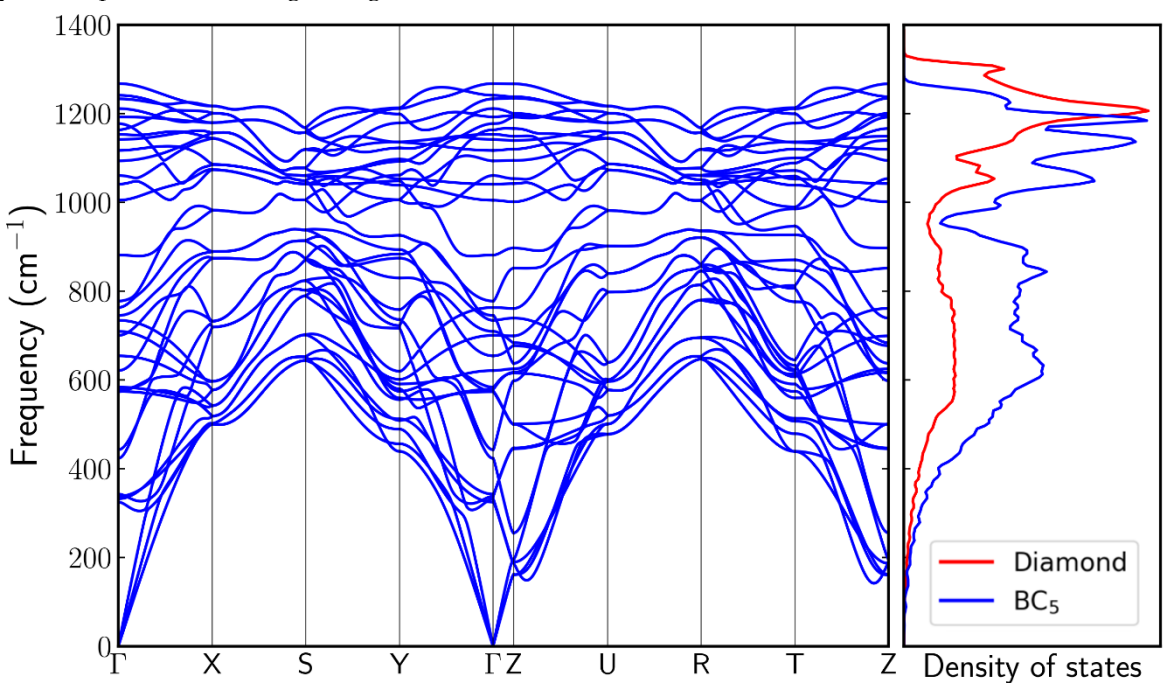
The corresponding simulated x-ray diffraction pattern is shown in Figure 8 and compared with that of the HBCC sample. We note that there exists another orthorhombic BC5 also with Pmma symmetry [6,9]; this structure with direct boron-boron bonding has slightly higher energy and a predominant x-ray diffraction peak below 10°, which is not observed in our experiments.



238

Figure 8: Theoretical x-ray diffraction patterns with wavelength 1.5406 angstrom (Cu K-alpha1) for orthorhombic BC₅ with Pmma symmetry compared to the experimental x-ray diffraction pattern for HBCC sample. Each spectrum is normalized by its highest peak intensity.

We also have performed DFT calculations to investigate the vibrational frequencies of superhard BC5 phases at zero pressure. Figure 9 shows the phonon dispersion and phonon density of states (DOS) of the orthorhombic BC5 structure in Figure 7. In Figure 9, there is no negative frequency mode identified in the spectra, showing that the theoretical BC5 structure in Figure 7 is dynamically stable. The phonon DOS of cubic diamond is also shown for comparison. The existence of boron atoms softens the chemical bonds and shifts the vibrational modes to lower frequencies as compared to those in diamond. We note that the pure GGA functional underestimates the vibrational frequencies by a few percent; a more accurate determination of the phonon energies can be obtained using for example the B3LYP hybrid functional [28], which however is computationally much more expensive. Figure 10 shows the theoretical Raman scattering spectra for diamond and BC₅ at zero pressure. The single theoretical Raman peak for diamond is located at 1294.7 cm⁻¹. For BC₅, two main theoretical Raman peaks are located at 1209.3 and 1174.7 cm⁻¹. Additional low-energy theoretical Raman peaks are located at 702.2 cm⁻¹ and 508.6 cm⁻¹. As shown in Table II, overall the theory and experiment are in good agreement.



260

Figure 9: Phonon dispersion and density of states (DOS) of orthorhombic BC5 with Pmma symmetry. The phonon DOS of cubic diamond is also shown. Each phonon DOS spectrum is normalized by its peak intensity.

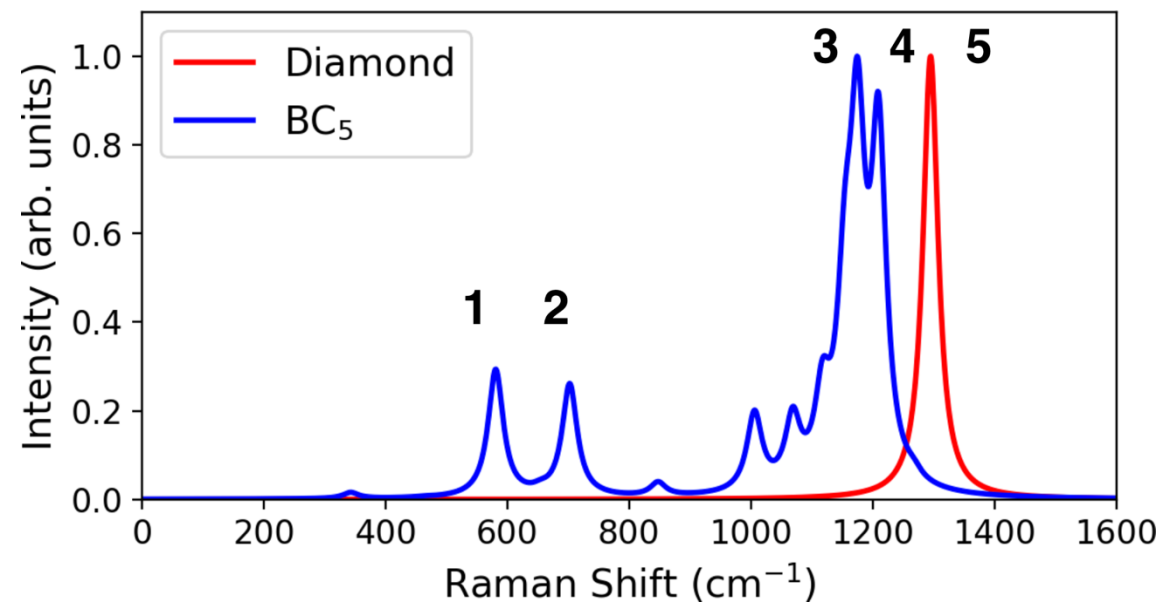
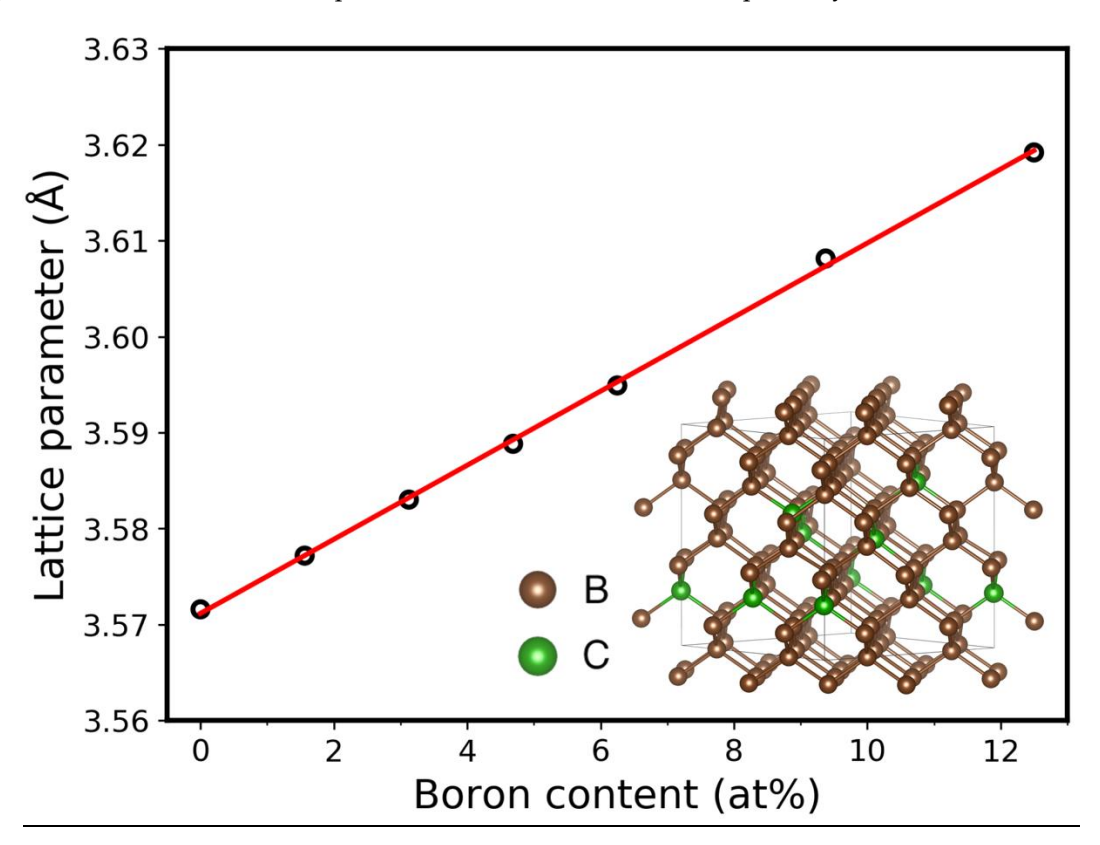


Figure 10: Comparison of the Raman spectrum for the cubic-diamond phase without boron incorporation and the orthorhombic BC5 with Pmma symmetry.

At a semi-quantitative level, our results show that the main vibrational frequency in BC_5 softens compared to that in cubic diamond due to slightly elongated atomic bonds, and that broad low-energy peaks emerge due to the presence of boron atoms [9]. These generic features are also observed in other superhard BC_5 phases and in good agreement with the experimental Raman measurements as shown in Figure 2.

Further DFT calculations were performed to estimate the lattice parameter of the cubic diamond structure as a function of at% boron doping. The calculation predicts that the lattice parameter linearly increases with increasing boron content, in accord with the Vegard's law [29]. Figure 11 shows the calculated points as well as a linear fit with equation y = 0.003859x + 3.5712.



<u>Figure 11</u>: Plot of DFT calculation showing lattice parameters for cubic diamond structure as a function of the boron content. The linear behavior is predicted by Vegard's Law. The inset structure shows a 2x2x2 supercell of boron-doped cubic diamond with boron content of 9.375 at%.

The DFT software Quantum-Espresso was used to allow unit cells or supercells of boron-doped diamond to relax using BFGS method while maintaining the restriction of the cubic diamond structure. The maximum lattice parameter measured by XRD of the thin films is 3.5917 Å. Using this value with the linear fit equation; the calculations predict a boron content of 5.3 at%. It should be added that our measured value of lattice parameter of 3.5917 Å is similar to 3.589 Å, the value reported for the cubic phase of BC $_3$ [30] and 3.59 Å, the value reported for the cubic phase of BC $_3$ [1]. This indicates that our HBCC film consists of highly doped diamond, containing 5.3 at% boron in a matrix of amorphous boron-doped graphitic carbon which accepts the remaining 7.7 at% boron, as measured by XPS.

4. Discussion

Aided by evolutionary algorithm predictions, we have synthesized a novel series of boron-carbon materials using microwave plasma chemical vapor deposition technique employing hydrogen/methane/diborane gas-phase chemistry. The hardness of the film can be varied from 8 GPa to as high as 62 GPa depending on the growth conditions, thus opening the door for superhard materials synthesis suitable for high temperature operations. We have used DFT calculations to explain our experimental results, achieving overall good theory-experiment agreements on the measured hardness and vibrational spectra recorded by Raman spectroscopy. The theoretically predicted stable orthorhombic structure for stoichiometric BC5 (16.7 at% boron) was not observed in our metastable synthesis from the gas-phase. Instead, we document a metastable cubic diamond-like phase all the way to the highest boron concentration of 7.7 at%. Our data analysis also indicates the lattice parameter of the cubic hard phase synthesized by microwave plasma method is similar to the hard phases reported in BC3 and BC5 materials that have been synthesized by high-pressure high-temperature techniques. Low pressure/low-temperature plasma synthesis from the gas phase of the superhard boron-carbon composites offer advantages over high-pressure high-temperature methods in terms of large area deposition on a variety of substrates.

- **Author Contributions:** Paul Baker and Yogesh Vohra conceived the plasma synthesis process for boron-carbon composites and carried out the growth experiments. Wei-Chih Chen and Cheng-Chien Chen contributed to theoretical calculations including evolutionary algorithm predictions and density functional theory of boron-carbon system. Sumner Harris carried out SEM, x-ray diffraction analysis and DFT calculations to predict boron-doped diamond lattice parameters, Aaron Catledge performed the nanoindentation hardness measurements and the related analysis. Kathryn Ham carried out the Raman spectroscopy on all samples and the related analysis. Yogesh Vohra coordinated the development of manuscript for publication.
- Funding: This material is based upon work supported by the National Science Foundation (NSF) EPSCoR RII-Track-1 Cooperative Agreement OIA-1655280. We also acknowledge support from the NSF Major Research Instrumentation (MRI) Grant No. DMR- 1725016. Any opinions, findings, and conclusions or recommendations expressed in this material are those of the author(s) and do not necessarily reflect the views of the National Science Foundation.
- Conflicts of Interest: The authors declare no conflict of interest. The funders had no role in the design of the study; in the collection, analyses, or interpretation of data; in the writing of the manuscript, and in the decision to publish the results.

319 References

- 320 1. Solozhenko, V. L.; Kurakevych, O. O.; Andrault, D.; Godec, Y. L.; Mezouar, M., Ultimate Metastable Solubility of Boron in Diamond: Synthesis of Superhard Diamondlike BC5. *PHYSICAL REVIEW LETTERS* 2009, 102 (1), 4.
- Calandra, M.; Mauri, F., High-Tc Superconductivity in Superhard Diamondlike BC₅. *Physical Review Letters* 2008, 101 (1), 016401.

- 325 3. Yao, Y.; Tse, J. S.; Klug, D. D., Crystal and electronic structure of superhard BC₅: First-principles structural optimizations. *Physical Review B* **2009**, *80* (9), 094106.
- 327 4. Jiang, C.; Lin, Z.; Zhao, Y., Superhard diamondlike BC₅: A first-principles investigation. *Physical Review B* 2009, *80* (18), 184101.
- 5. Lazar, P.; Podloucky, R., Mechanical properties of superhard BC₅. *Applied Physics Letters* **2009**, 94 (25), 251904.
- 6. Li, Q.; Wang, H.; Tian, Y.; Xia, Y.; Cui, T.; He, J.; Ma, Y.; Zou, G., Superhard and superconducting structures of BC₅. *Journal of Applied Physics* **2010**, *108* (2), 023507.
- 7. Zhao, W. J.; Wang, Y. X., Mechanical properties of superhard diamondlike BC₅. *Solid State Communications* **2011**, *151* (6), 478-481.
- 335 8. Li, M. M.; Xiaofeng, F.; Zheng, W. T., First-principle calculations on the structural stability and electronic properties of superhard B x C y compounds. *Journal of Physics: Condensed Matter* **2013**, 25 (42), 425502.
- 9. Alp, I. O.; Ciftci, Y. O., Physical Properties of Superhard Diamond-Like BC5 from a First-Principles Study. *Journal of Electronic Materials* **2018**, 47 (1), 272-284.
- 339 10. Baker, A. P.; Goodloe, R. D.; Vohra, K. Y., Morphological Transition in Diamond Thin-Films Induced by Boron in a Microwave Plasma Deposition Process. *Materials* **2017**, *10* (11).
- 341 11. Oganov, A. R.; Glass, C. W., Crystal structure prediction using ab initio evolutionary techniques: Principles and applications. *The Journal of Chemical Physics* **2006**, *124* (24), 244704.
- 343 12. Glass, C. W.; Oganov, A. R.; Hansen, N., USPEX—Evolutionary crystal structure prediction. *Computer Physics Communications* **2006**, *175* (11), 713-720.
- 345 13. Lyakhov, A. O.; Oganov, A. R.; Stokes, H. T.; Zhu, Q., New developments in evolutionary structure prediction algorithm USPEX. *Computer Physics Communications* **2013**, *184* (4), 1172-1182.
- 347 14. Kresse, G.; Furthmüller, J., Efficiency of ab-initio total energy calculations for metals and semiconductors using a plane-wave basis set. *Computational Materials Science* **1996**, *6* (1), 15-50.
- 349 15. Kresse, G.; Furthmüller, J., Efficient iterative schemes for ab initio total-energy calculations using a plane-wave basis set. *Physical Review B* **1996**, *54* (16), 11169-11186.
- 351 16. Blöchl, P. E., Projector augmented-wave method. *Physical Review B* **1994**, *50* (24), 17953-17979.
- 352 17. Kresse, G.; Joubert, D., From ultrasoft pseudopotentials to the projector augmented-wave method. *Physical Review B* **1999**, *59* (3), 1758-1775.
- 354 18. Perdew, J. P.; Burke, K.; Ernzerhof, M., Generalized Gradient Approximation Made Simple. *Physical Review Letters* **1996**, 77 (18), 3865-3868.
- 356 19. Monkhorst H. J.; Pack J. D., Special points for Brillouin-zone integrations. Physical Review B 1976, *13* (12), 5188–5192.
- 358 20. Gonze, X.; Lee C., Dynamical matrices, Born effective charges, dielectric permittivity tensors, and interatomic force constants from density-functional perturbation theory. *Physical Review B* **1997**, *55* (*16*), 10355.
- Togo, A.; Tanaka, I., First principles phonon calculations in materials science. *Scripta Materialia* 2015, 108,
 1-5.
- 22. Chen, X.-Q.; Niu, H.; Li, D.; Li, Y., Modeling hardness of polycrystalline materials and bulk metallic glasses. Intermetallics **2011**, *19* (9), 1275-1281.
- 365 23. Ager, J. W.; Walukiewicz, W.; McCluskey, M.; Plano, M. A.; Landstrass, M. I., Fano interference of the Raman phonon in heavily boron-doped diamond films grown by chemical vapor deposition. *Applied Physics Letters* **1995**, 66 (5), 616-618.
- 368 24. May, P. W.; Ludlow, W. J.; Hannaway, M.; Heard, P. J.; Smith, J. A.; Rosser, K. N., Raman and conductivity studies of boron-doped microcrystalline diamond, facetted nanocrystalline diamond and cauliflower diamond films. *Diamond and Related Materials* 2008, 17 (2), 105-117.
- Warren, J. L.; Yarnell, J. L.; Dolling, G.; Cowley, R. A., Lattice Dynamics of Diamond. *Physical Review* **1967**, 158 (3), 805-808.
- 26. Lyakhov, A. O.; Oganov, A. R., Evolutionary search for superhard materials: Methodology and applications to forms of carbon and TiO2, *Physical Review B* **2011**, *84* (9), 092103.
- 375
 27. Šimůnek, A.; Dušek, M., Generalized bond-strength model of Vickers hardness: Application to Cr4B, CrB,
 376
 CrB2, CrB4, Mo2B, MoB2, OsB2, ReB2, WB2, WB3 and Ti1.87B50, Mechanics of Materials 2017, 112, 71.

383

384

385

- 377 28. Baima, J.; Zelferino, A.; Olivero, P.; Erba, A.;Dovesi, R., Raman spectroscopic features of the neutral vacancy in diamond from ab initio quantum-mechanical calculations. *Physical Chemistry Chemical Physics* 379 2016, *18* (3), 1961-1968.
- 380 29. Vegard, L., Die Konstitution der Mischkristalle und die Raumfüllung der Atome. Zeitschrift für Physik 1921, 5 (1), 17.3
 - 30. Zinin, P. V.; Ming, L. C.; Ishii, H. A.; Jia, R.; Acosta, T.; Hellebrand, E., Phase transition in BCx system under high-pressure and high-temperature: Synthesis of cubic dense BC₃ nanostructured phase. *Journal of Applied Physics* **2012**, *111* (11), 114905.